

Acoustic full-waveform tomography of realistic 2D synthetic seismic elastic data

Damodara Nara^{1,*} and Kalachand Sain²

¹CSIR-National Geophysical Research Institute, Uppal Road, Hyderabad 500 007, India

²Wadia Institute of Himalayan Geology, Dehradun 248 001, India

Advanced computing facilities accelerate the research in highly computational seismic imaging techniques (full-waveform tomography (FWT) and migration) that play a vital role in hydrocarbon exploration. We have carried out a synthetic study to understand the practical intricacies of FWT for its successful application to field seismic data by choosing different strategies. The results show that the high-resolution features, which are missing from the conventional traveltime tomography, are well imaged by the FWT. Further, frequency overlapping is more suitable than discrete frequencies without overlapping for FWT in obtaining reasonable results from multiscale imaging.

Keywords: Elastic and acoustic data, frequency domain, hydrocarbon exploration, ocean-bottom seismometer, waveform tomography.

SEVERAL theoretical studies on full-waveform tomography (FWT) have been carried out over the past 20 years. However, most of its applications lie in the theoretical domain because of the complexity involved in understating and implementing the physics of seismic waves. FWT computes the difference between observed and synthetic responses and updates the current velocity models, similar to reverse time migration (RTM) of the residual dataset, by computing the gradient volume^{1,2}. An excellent technical review of FWT is given by Virieux and Operto³.

Implementation of the FWT algorithm and its strategies for field seismic data is more difficult than the synthetic data. To understand the practical aspects of FWT, we must study the sensitivities of different factors such as the starting model, frequency selection and their overlapping in multiscale imaging in frequency-domain FWT. Here, we have carried out a synthetic study to understand the intricacies involved in FWT of field seismic data (Figure 1). In addition, one must keep in mind that the FWT is sensitive to other factors that include the algorithm which has been implemented, solution of the inverse problem, cost function, step-length criteria, etc. However, these factors are beyond the scope of the present study, and need further attention in future research.

Forward modelling

We constructed a two-dimensional P -wave velocity (V_p) model by correlating two available sonic logs in a marine environment (Figure 2 *a*). The true model shows very fine details of the subsurface and is complex in nature. This can be considered as one of the benchmark models for research in seismic tomography. The S -wave velocity (V_s) and density (ρ) models can be derived from the V_p model using eqs (1) and (2) (Figure 2 *b* and *c*).

$$V_s \text{ (m/s)} = 0.8619 \times V_p - 1172, \quad (1)$$

$$\rho \text{ (g/cc)} = 0.31 \times (V_p)^{0.25}. \quad (2)$$

The dimensions of the model are 50.0 km in length and 5.0 km in depth. It is parameterized by $12,500 \times 1250$

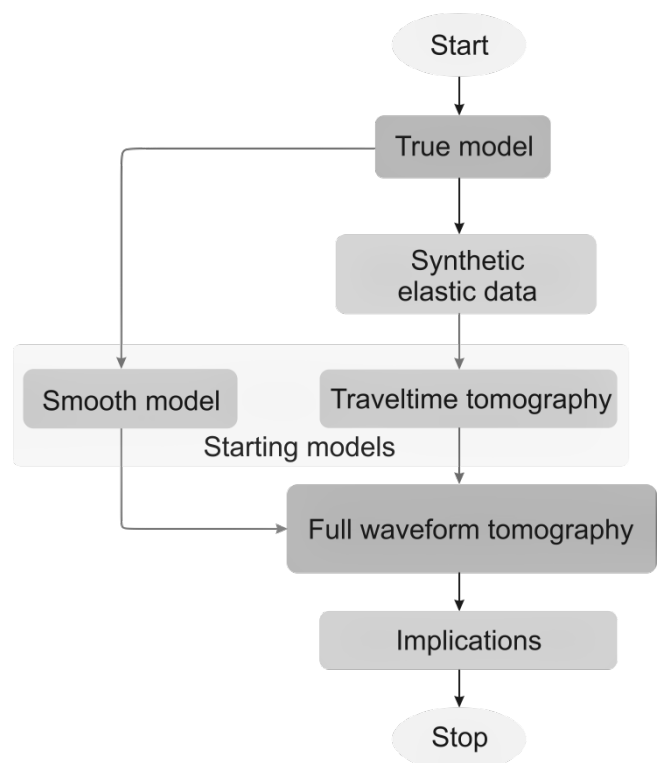


Figure 1. Flowchart of the acoustic full-waveform tomography (FWT) from elastic synthetic data.

*For correspondence. (e-mail: naradamu@gmail.com)

nodes for forward modelling using 4 m grid spacing, which may be sufficient to represent the true model. However, the model has very fine-scale structural details in the order of log-scale. One can notice two important dominant features: (i) high-velocity pinch-out and (ii) dominant convex features at a depth of 3.0 and 4.0 km respectively, with an intermediate hidden zone between them. Also, in Figure 2, we have marked the major interfaces observed in the model. The wide-angle elastic data were generated using the finite-difference modelling for such a complex geological model^{4,5}. The synthetic seismic experiment includes a total of 51 ocean bottom seismometers (OBSs) at 1.0 km spacing, and 1000 shots (at 5 m below the water surface) per OBS with 50 m interval. The OBS depth varies from a minimum of 45 m to the maximum of 370 m. The normalized Ricker wavelet with central frequency 10 Hz was used to generate the synthetic data. The total recording length was 16.384 s with a sampling interval of 4 ms. Figure 3 shows a representative OBS gather with a reduction velocity 6.0 km/s. Hereafter, the generated elastic data are referred to as the realistic seismic data throughout this study.

Visco-acoustic full-waveform tomography

We applied visco-acoustic FWT in the frequency domain to the realistic seismic data by choosing different strategies while selecting the starting model and/or inverted frequencies^{6–9}. The FWT algorithm solves the frequency-domain wave equation using mixed-grid finite-difference approach during forward modelling phase¹⁰ and uses the

classic gradient method to solve the weighted least square linearized inverse problem¹¹.

Starting model

For any gradient search inversion, we need a starting model. We have developed the starting model from two different approaches: (i) smoothed version of the true model and (ii) first-arrival traveltimes tomography model. The first approach is straightforward, and is generally used to demonstrate the efficacy of seismic tomography during the development of an inversion algorithm. For field experiments the true velocity structure is not known; however, many researchers prefer to use only the smooth version of the true model. This avoids the situation of developing an initial model from synthetic data as in field experiments using practical approaches (e.g. first arrival/reflection traveltimes tomography, stereo-tomography, etc.). The second approach is considered for field applications in which the subsurface model is unknown. We have focused on both types of initial models in this study.

We employed the well-known first-arrival seismic tomography (FAST) code to traveltimes data picked from all OBSs^{12,13}. This package offers iterative regularized inversion in terms of data misfit and roughness, and calculates new ray paths at each iteration. For more details, the reader may refer to the literature^{14–16}. A total of 50,903 first-arrival picks with 30 ms uncertainty were used. We parameterized the model in 201×21 grids having 0.25×0.25 km grid size in forward modelling and 0.5×0.25 km cell size during inversion. The final traveltimes tomographic model was achieved after 16 iterations with root mean square traveltimes residual of 33.8 ms from a starting model that was derived using the intercept-time method from different OBS data and juxtaposing them¹⁶ (Figure 4). Figure 5 shows the corresponding ray paths for the final model and traveltimes residual plots for both starting and final models. The ray paths plot clearly shows that there is good ray coverage and penetration up to a depth of ~ 3.5 – 4.0 km (Figure 5 a). Also, there is no ray penetration at the corners of the profile. This indicates that the delineated model has good confidence at the ray-penetrated

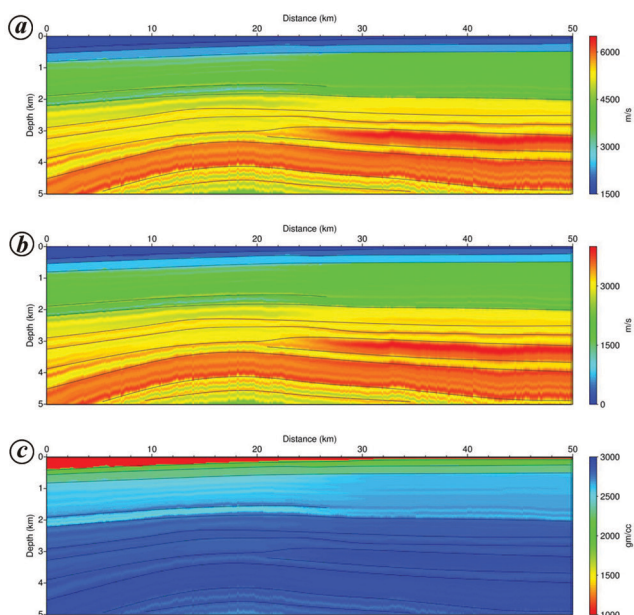


Figure 2. (a) True P -wave velocity (V_p), (b) S -wave velocity (V_s) models and (c) density model used for generating elastic data. Identified major interfaces are shown by thin black lines.

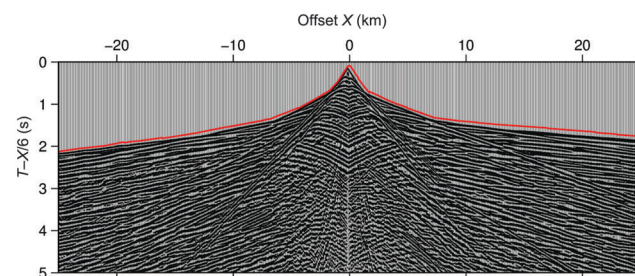


Figure 3. A representative ocean bottom seismometer (OBS) gather displayed with a reduction velocity of 6.0 km/s. The picked first-arrivals are superimposed on the OBS gather.

positions (Figure 4 *b*); the remaining positions represent the background model only. This traveltime tomography (TT) model was used as one of the starting models for FWT. It allows the inherent numerical propagation error during the synthetic data generation similar to real field seismic data acquisition. The other starting model is the smoothed version of the true model that has been ob-

tained by applying damped least square moving average filter on the true model (Figure 6). The dimensions for the moving average filter in both distance and depth are 50 and 50 samples respectively. Both the starting models show the long-wavelength features but lack in finer details (Figures 4 *b* and 6), and we expect these from FWT.

Data pre-processing

Since we apply acoustic FWT, data pre-processing is necessary to mitigate or exclude arrivals and propagation effects in data which cannot be predicted from acoustic approximation. A time window of 1300 ms was applied around the first arrivals to exclude the non-acoustic arrivals such as the P-SV converted arrivals, free-surface multiples and early ambient noise. Figure 7 displays a representative pre-processed OBS gather. The data were subsequently Fourier-transformed and the selected components were extracted in order to form a mono-frequency dataset for FWT in the frequency domain.

Full-waveform tomography

Many of the past case studies have verified that a discrete set of a few frequencies is enough to obtain reasonable results from FWT in the frequency domain¹⁷⁻¹⁹. Earlier studies followed two strategies: (i) discrete set of frequencies with an equal interval^{6,8,20,21}, and (ii) discrete set of frequencies selected by the criteria of Sirgue and Pratt²². We briefly describe the later strategy below.

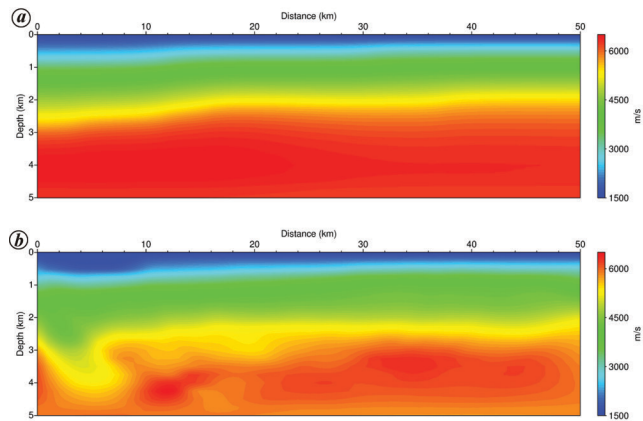


Figure 4. (a) Starting model and (b) final velocity model from first-arrival traveltime tomography.

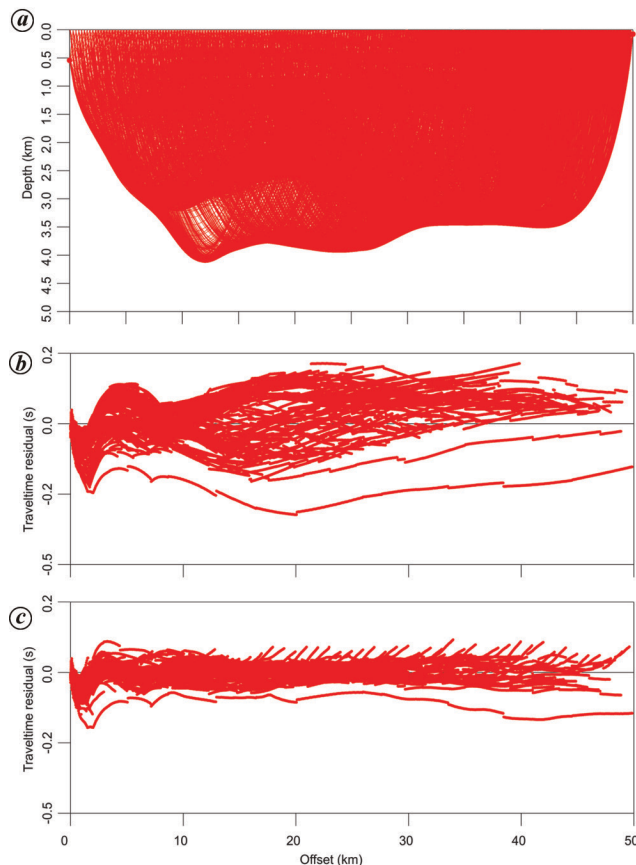


Figure 5. *a*, Ray tracing through the final traveltime tomographic model. Traveltime residual for (b) starting and (c) final models respectively.

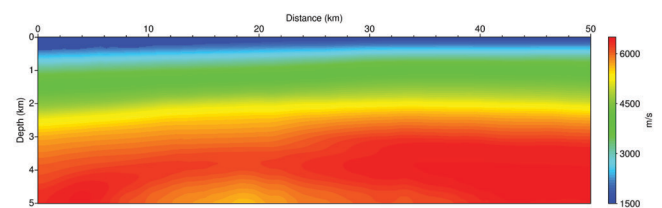


Figure 6. Smoothed version of the true model achieved by applying damped least squares moving average filter on the model. The dimensions for the moving average in both distance and depth are 50 and 50 samples respectively.

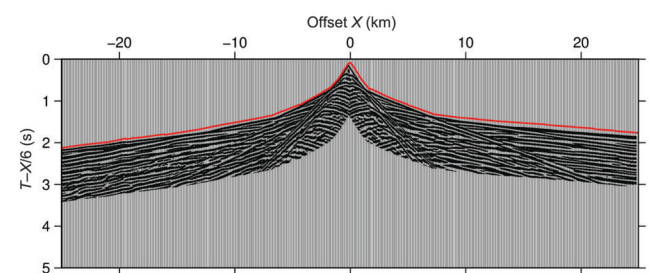


Figure 7. A representative pre-processed OBS gather displayed with a reduction velocity of 6.0 km/s. The picked first arrivals are superimposed on the OBS gather.

Frequency selection criteria: As the computational cost increases over a range of frequencies starting from low to high frequency in FWT, Sirgue and Pratt²² have demonstrated that a properly selected, limited number of frequencies is sufficient for utilization of the wavenumber spectrum. Brenders and Pratt¹⁸ considered FWT using the selected frequencies²² as an efficient strategy. It has been applied to numerous studies by Brenders and Pratt¹⁸, and Wang and Rao¹⁹. We also adopted a similar strategy in the visco-acoustic FWT. For continuous wavenumber coverage, the proposed strategy for frequency discretization is

$$f_{n+1} = \frac{f_n}{\alpha}, \tag{3}$$

where f_n is the previous frequency, f_{n+1} the new frequency for inversion and α is the cosine of the maximum incident angle for a scattered wavefield, corresponding to the maximum value of half source–receiver offset h_{\max} and target depth z .

$$\alpha = \frac{z}{\sqrt{h_{\max}^2 + z^2}}. \tag{4}$$

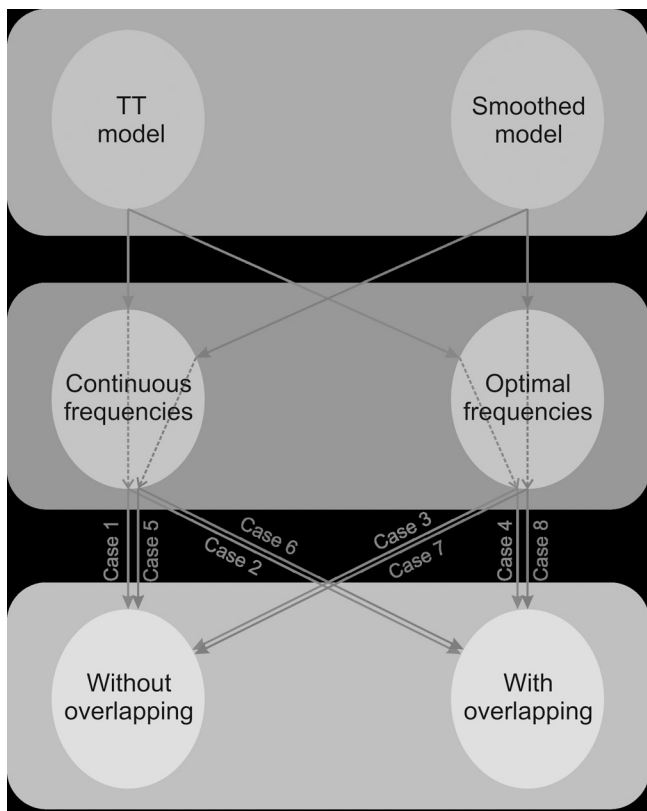


Figure 8. Flowchart for different strategies of FWT. Case 1: TT model – continuous frequency set without overlapping. Case 2: TT model – continuous frequency set with overlapping. Case 3: TT model – optimal frequency set without overlapping. Case 4: TT model – optimal frequency set with overlapping. Case 5: Smooth model – continuous frequency set without overlapping. Case 6: Smooth model – continuous frequency set with overlapping. Case 7: Smooth model – optimal frequency set without overlapping. Case 8: Smooth model – optimal frequency set with overlapping.

Results and discussion

Since our focus is to study the influence of the starting model and frequency selection and their combinations in producing the best possible results from visco-acoustic FWT in the frequency domain, we restricted using the same FWT parameters in each case. Figure 8 summarizes the different cases where the models differ from each other during multiscale imaging. Further, we have used constant density and quality factor (Q) for all case studies. Kurzman *et al.*²³ showed that for single-parameter acoustic inversion, the constant density and Q models are sufficient to obtain better results from FWT. The case studies are described below.

Case 1: TT model – continuous frequency set without overlapping

In this case, the TT model as the starting model and continuous discrete set of total 40 frequencies starting from 2 to 21.5 Hz with an interval 0.5 Hz were used. These 40 frequencies formed 20 groups (group 1, 2, 2.5 Hz; group 2, 3.0, 3.5 Hz; group 3, 4.0, 4.5 Hz, ...) each having two frequencies, without any overlapping between the groups.

Case 2: TT model – continuous frequency set with overlapping

We used the same starting model and discrete set of frequencies as in case 1, but formed 39 groups by overlapping between the frequency groups with one common frequency (group 1, 2, 2.5 Hz; group 2, 2.5, 3.0 Hz; group 3, 3.0, 3.5 Hz, ...).

Case 3: TT model – optimal frequency set without overlapping

We used the same starting model as in cases 1 and 2, and the frequency selection was done using the criterion of Sirgue and Pratt²². According to this criterion, only two frequencies, viz. 2.0 and 10.2 Hz within our range of interest between 2.0 and 20.0 Hz will contribute. To maintain consistency in the frequency range and stabilize the inversion, we added four more frequencies (1.95, 19.54, 20.03 and 20.1 Hz) and then inverted independently all six frequencies one after another (1.95, 2.0, 10.2, 19.54, 20.03 and 20.1 Hz) without overlapping.

Case 4: TT model – optimal frequency set with overlapping

Same strategy as used in case 3, except for frequency overlapping. We formed all six frequencies into four groups with each group having three frequencies by overlapping

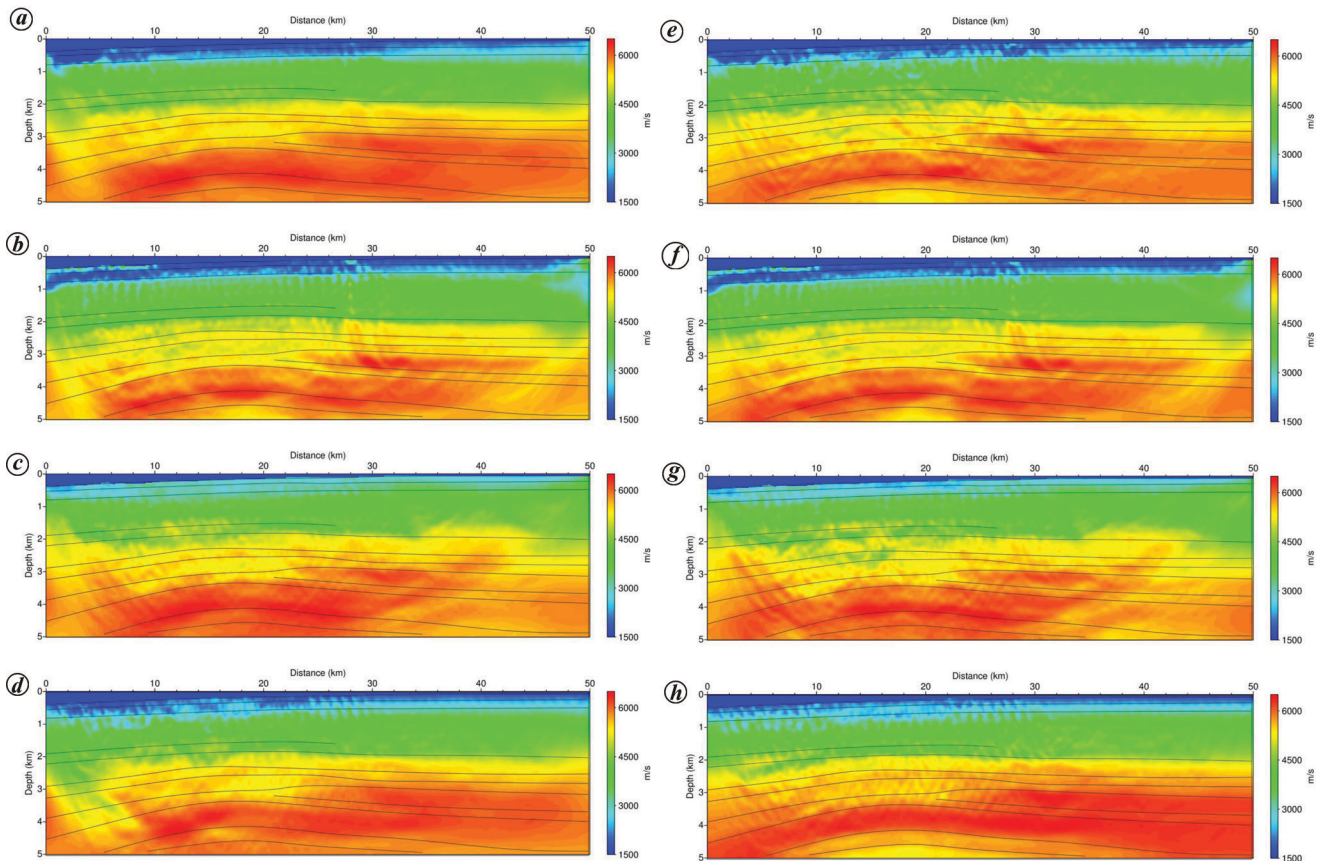


Figure 9. Final FWT models obtained from each case as described in Figure 8. Major interfaces are superimposed on the final FWT models. *a*, Case 1; *b*, case 2; *c*, case 3; *d*, case 4; *e*, case 5; *f*, case 6; *g*, case 7; *h*, case 8.

between the groups (group 1, 1.95, 2.0, 10.2 Hz; group 2, 2.0, 10.2, 19.54 Hz; group 3, 10.2, 19.54, 20.03 Hz; group 4, 19.54, 20.03, 20.1 Hz).

Case 5 (smooth version of true model – continuous frequency set without overlapping), case 6 (smooth version of true model – continuous frequency set with overlapping), case 7 (smooth version of true model – optimal frequency set without overlapping) and case 8 (smooth version of true model – optimal frequency set with overlapping) were similar to case 1, case 2, case 3 and case 4 respectively, except for the starting model which was the smoothed version of the true model.

Figure 9 shows the final models, obtained from FWT for each case as described in Figure 8. The one-dimensional velocity–depth functions extracted from the FWT models at two different positions, viz. 17.9 and 28.9 km distance were compared with those extracted from the true model generated from well-log data (Figure 10).

In general, we need good correlation with the available well-log data to confirm that the models are reliable to interpret/postulate further about the subsurface in terms of geological features. However, this may lead us in the wrong direction as we will be observing the 1D velocity–depth functions at two well positions (17.9 and 28.9 km)

(Figure 10). All 1D velocity–depth functions of FWT are almost close enough (at least 60%–70%) to the true models at both well positions, except at a few depth positions. Expecting an excellent correlation with a well-log is also not fair due to several factors such as usage of band-limited data, discrete frequency inversion, difference between the log and seismic scale and many others. Note that we have performed FWT with consistent parameters such as both modelling and inversion for each FWT case. This may terminate updating of the FWT model before the maximum number of iterations due to deterministic stopping rule. It may also affect inherently the model update, irrespective of the initial model used for FWT.

All the final 2D velocity models obtained from FWT help delineate the finer details and major interface structures, which are clearly absent in the TT tomography models (Figure 9). However, these FWT models are not sufficient to explain all the finer details present in the true model. This may be due to nonlinearity of the problem, acoustic approximations, sufficient band-limiting, discrete frequency selection and many inherent unexplainable problems. These models can be further improved by pursuing FWT with more number of iterations and including higher frequencies. However, in reality, one does not know

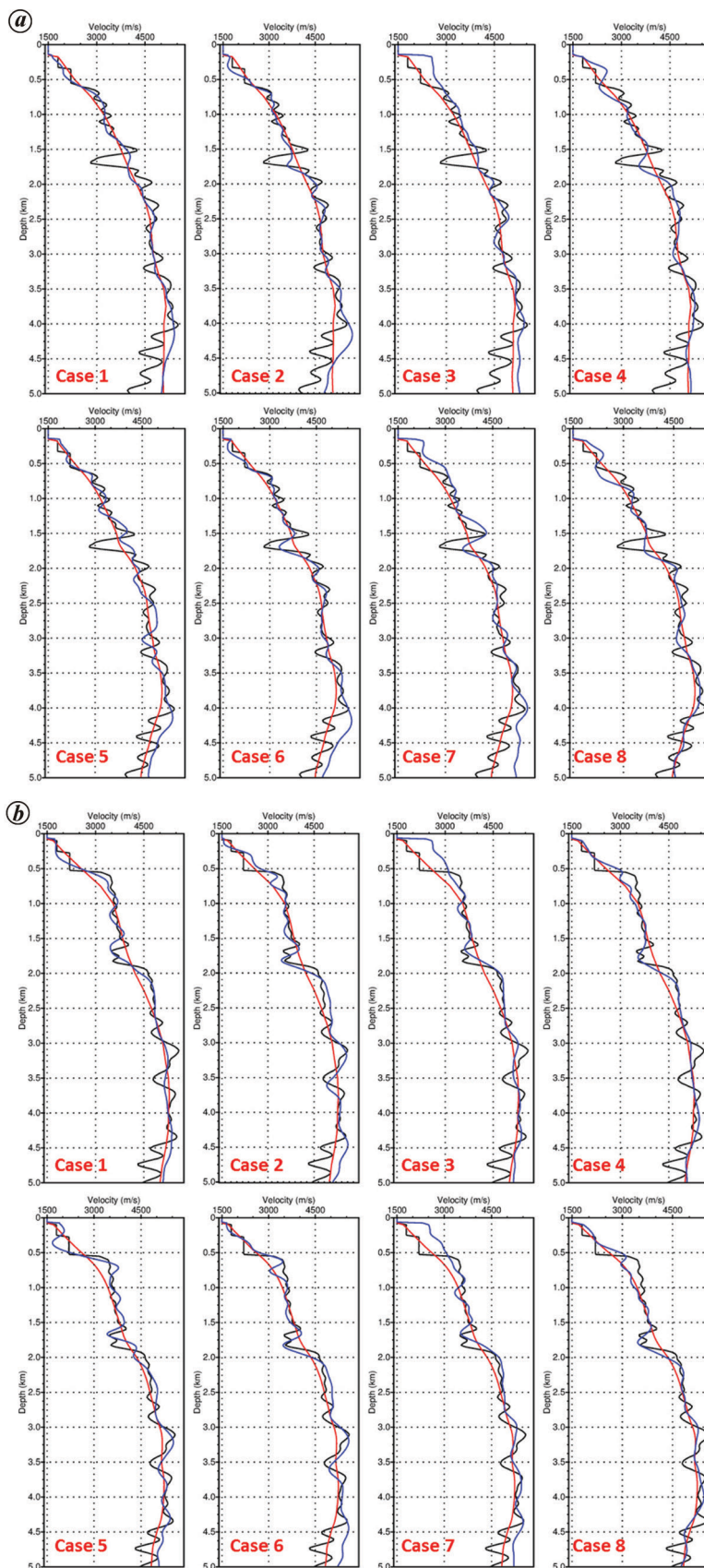


Figure 10. One-dimensional models extracted from the true (black), traveltime tomography (red) and FWT (blue) models from each case at (a) 17.9 km and (b) 28.9 km.

the subsurface structure, but derives the velocity model from the acquired seismic data that are band-limited and may not be sufficient to resolve all finer details in the order of log scale, even though one performs sophisticated FWT. Hence, we will always get a relatively larger wavelength velocity model from field seismic data than that obtained from the well-log data.

Thus, considering all these situations, 1D velocity model comparisons (Figure 10) and 2D velocity models (Figure 9), we observe that the models obtained in case 2 and case 6 are in good correlation with one another and maintain consistency in delineating the major structural features of the true model. We can draw some important conclusions in obtaining optimum solution from the acoustic FWT. Irrespective of the initial model, overlapping of the frequencies produces reliable results. As discussed earlier, the inherent error of the initial model, constructed from any other practical approach will take advantage of examining the algorithm's capability rather than smoothed version of the true model. Further, this explains the complexities in the application of acoustic FWT with real field seismic data during the delineation of fine-scale details for different applications, such as reservoir characterization, etc. This also suggests that the interpreters need to carefully consider the FWT models with maximum possible prior information due to the well-log details, which are confined to a single position in the profile.

Conclusion

Though FWT has been applied to a limited number of field seismic data, the tool mostly lies in the theoretical domain to understand the intricacies during multiscale imaging. We studied the role of the starting model and choice of frequency in acoustic FWT from elastic wide-angle synthetic data that have been generated for a realistic model, obtained from well logs. Since FWT is highly computational-intensive, such synthetic case studies are useful to understand the practical issues for successful application to field seismic data. This study suggests that overlapping of frequency groups with continuous interval always produces the best possible results, irrespective of the starting model. To demonstrate the capability of the FWT algorithm, many researchers use the smooth version of the true model as the starting model, and reach the solution without much difficulty. However, it may not be possible to have such a close starting model in all real-time scenarios. Further, it provides flexibility to avoid the inherent propagation of errors in the model. In such a situation, the TT model or any other model that can be derived from the data can be used as the best possible starting model in demonstrating the efficacy of the FWT algorithm. While using the smooth version of the true model as the starting model, one should allow sufficient smooth-

ing filter by which one can develop a model similar to a model that can be obtained by any practical approach (e.g. first arrival/reflection traveltime tomography, stereotomography).

Although the FWT models show detailed velocity structure than the TT model, some finer details are missed in the FWT models. This may be due to the application of acoustic modelling to realistic elastic data, use of a discrete set of frequencies and, most importantly, inadequacy of wide-angle synthetic seismic data to resolve subsurface finer details in the order of log scale. One can recover the true model from FWT of wide-angle synthetic seismic data only when the true model is close to seismic scale or greater the log scale that has been used here. These types of studies play a key role in highly computational imaging techniques that take a long duration to produce the best possible results within the timeframe. The usage of variable grid sizes is also helpful in multiscale imaging techniques to save the computational time, which needs to be further studied.

1. Lailly, P., The seismic inverse problem as a sequence of before stack migrations. In *Conference on Inverse Scattering – Theory and Application* (eds Bednar, J. B. *et al.*), Society for Industrial and Applied Mathematics (SIAM), Philadelphia, USA, 1983, pp. 206–220.
2. Tarantola, A., Inversion of seismic reflection data in the acoustic approximation. *Geophysics*, 1984, **49**, 1259–1266.
3. Virieux, J. and Operto, S., An overview of full waveform inversion in exploration geophysics. *Geophysics*, 2009, **74**, WCC127–WCC152.
4. Bohlen, T., Interpretation of measured seismograms by means of visco-elastic finite difference modeling. Ph.D. thesis, Kiel University, Germany, 1998.
5. Bohlen, T., Parallel 3-D viscoelastic finite-difference seismic modeling. *Comput. Geosci.*, 2002, **28**(8), 887–899.
6. Dessa, J. X., Operto, S., Kodaira, S., Nakanishi, A., Pascal, G., Virieux, J. and Kaneda, Y., Multiscale seismic imaging of the eastern Nankai trough by full waveform inversion. *Geophys. Res. Lett.*, 2004, **31**, L18606.
7. Operto, S., Ravaut, C., Improta, L., Virieux, J., Herrero, A. and Dell'Aversana, P., Quantitative imaging of complex structures from dense wide-aperture seismic data by multiscale traveltime and waveform inversions: a case study. *Geophys. Prospect.*, 2004, **52**, 625–651.
8. Operto, S., Virieux, J., Dessa, J. X. and Pascal, G., Crustal seismic imaging from multifold ocean bottom seismometer data by frequency-domain full-waveform tomography: application to the eastern-Nankai trough. *J. Geophys. Res.*, 2006, **111**, B09306.
9. Ravaut, C., Operto, S., Improta, L., Virieux, J., Herrero, A. and Dell'Aversana, P., Multiscale imaging of complex structures from multifold wide-aperture seismic data by frequency-domain full-waveform tomography: application to a thrust belt. *Geophys. J. Int.*, 2004, **159**, 1032–1056.
10. Hustedt, B., Operto, S. and Virieux, J., Mixed-grid and staggered-grid finite-difference methods for frequency-domain acoustic wave modeling. *Geophys. J. Int.*, 2004, **157**, 1269–1296.
11. Pratt, R. G., Shin, C. and Hicks, G. J., Gauss–Newton and full Newton methods in frequency-space seismic waveform inversion. *Geophys. J. Int.*, 1998, **133**, 341–362.
12. Zelt, C. A., FAST – program package for first arrival seismic tomography, Rice University, Houston, 1998.

13. Zelt, C. A. and Barton, P. J., Three-dimensional seismic refraction tomography: a comparison of two methods applied to data from the Faeroe Basin. *J. Geophys. Res.*, 1998, **103**, 7187–7210.
14. Zelt, C. A., Sain, K., Naumenko, J. V. and Sawyer, D. S., Assessment of crustal velocity models using seismic refraction and reflection tomography. *Geophys. J. Int.*, 2003, **153**, 609–626.
15. Vijaya Rao, V., Damodara, N., Sain, K., Sen, M. K., Murty, A. S. N. and Sarkar, D., Upper crust of the Archean Dharwar Craton in southern India using seismic refraction tomography and its geotectonic implications. *Geophys. J. Int.*, 2015, **200**, 652–663.
16. Damodara, N., Vijaya Rao, V., Kalachand Sain, Prasad, A. S. S. R. S. and Murty, A. S. N., Basement configuration of the West Bengal sedimentary basin, India as revealed by seismic refraction tomography: its tectonic implications. *Geophys. J. Int.*, 2017, **208**, 1490–1507.
17. Brenders, A. J. and Pratt, R. G., Full waveform tomography for lithospheric imaging: results from a blind test in a realistic crustal model. *Geophys. J. Int.*, 2007, **168**, 133–151.
18. Brenders, A. J. and Pratt, R. G., Efficient waveform tomography for lithospheric imaging: implications for realistic 2D acquisition geometries and low frequency data. *Geophys. J. Int.*, 2007, **168**, 152–170.
19. Wang, Y. and Rao, Y., Reflection seismic waveform tomography. *J. Geophys. Res.*, 2009, **114**, B03304.
20. Malinowski, M. and Operto, S., Quantitative imaging of the Permo-Mesozoic complex and its basement by frequency domain waveform tomography of wide-aperture seismic data from the Polish Basin. *Geophys. Prospect.*, 2008, **56**, 805–825.
21. Gorszczyk, A., Operto, S. and Malinowski, M., Towards a robust workflow for deep crustal imaging by FWI of OBS data: the eastern Nankai trough revisited. *J. Geophys. Res.*, 2017, **122**(6), 4601–4630.
22. Sirgue, L. and Pratt, R. G., Efficient waveform inversion and imaging: a strategy for selecting temporal frequencies. *Geophysics*, 2004, **69**, 231–248.
23. Kurzmann, A., Przebindowska, A., Kohn, D. and Bohlen, T., Acoustic full waveform tomography in the presence of attenuation: a sensitivity analysis. *Geophys. J. Int.*, 2013, **195**(2), 985–1000.
24. Wessel, P. and Smith, W. H. P., New improved version of generic mapping tools released. *EOS, Trans. AGU*, 1998, **79**(47), 579.

ACKNOWLEDGEMENTS. We thank the Director, CSIR-National Geophysical Research Institute (NGRI), Hyderabad for permission to publish this paper (ID: NGRI/Lib/2021/Pub-155); the developers of different modelling and inversion open source packages used in this study, and P. Wessel and W. H. P. Smith²⁴ for the Generic Mapping Tools software used for plotting some of the figures. We also thank Prof. Mrinal K. Sen for a constructive interaction that helped improve the manuscript. D.N. thanks Department of Science and Technology, New Delhi for the INSPIRE Faculty Fellowship. This is a contribution to scientific research of CSIR-NGRI under MLP-6402-28(NS) and GAP-822-28(ND).

Received 24 January 2022; revised accepted 8 April 2022

doi: 10.18520/cs/v122/i12/1407-1414
